Journal of Sound and Vibration 327 (2009) 92–108

Contents lists available at ScienceDirect

Journal of Sound and Vibration

journal homepage: www.elsevier.com/locate/jsvi

# Numerical issues concerning the wave and finite element method for free and forced vibrations of waveguides

Y. Waki, B.R. Mace *, M.J. Brennan

*Institute of Sound and Vibration Research, University of Southampton, Highfield, Southampton SO17 1BJ, UK*

ARTICLE INFO

*Article history:*
Received 2 December 2008
Received in revised form
20 May 2009
Accepted 2 June 2009
Handling Editor: C.L. Morfey
Available online 30 June 2009

ABSTRACT

The wave and finite element (WFE) method is a numerical approach to the calculation of the wave properties of structures of arbitrary complexity. The method starts from a finite element (FE) model of only a short segment of the structure, typically by using existing element libraries and commercial FE packages. The dynamic stiffness matrix of the segment is obtained, a periodicity condition applied and an eigenvalue problem formed whose solution gives the dispersion equations and wave mode shapes. These define a wave basis from which the forced response can be found straightforwardly. Although straightforward in application, the WFE method is prone to numerical difficulties. These are discussed in this paper and methods to avoid or remove them described. Attention is focused on 1-dimensional waveguide structures, for which numerical problems are most severe. Three ways of phrasing the eigenvalue problem for free wave propagation are presented and a method based on singular value decomposition is proposed to determine eigenvectors at low frequencies. Discretisation errors are seen to occur if the segment is too large, while round-off errors occur if the segment is too small. This can be overcome by forming a super-segment from the concatenation of two or more segments. The forced response is then considered. The use of a reduced wave basis removes many problems. Direct calculation of the waves excited by a point force is very prone to poor numerical conditioning but can be circumvented by exploiting the orthogonality of the left and right eigenvectors. Numerical examples are presented.



## 1. Introduction

The propagation of waves in structures is of interest for many applications, especially at higher frequencies. Examples include the transmission of structure-borne sound, shock response and statistical energy analysis. Knowledge of the dispersion relations, group velocity, reflection and transmission characteristics etc., enables predictions to be made of disturbance propagation, energy transport and so on. This is true both for 1-dimensional waveguides, which are homogeneous in one dimension, but whose cross-section may have arbitrary complexity, and also for structures such as plates which are homogeneous in two dimensions, but whose properties may vary in an arbitrary manner through the thickness.

In simple cases, analytical expressions for the dispersion equation can be found (e.g. [1,2]). Examples include 1-dimensional structures such as thin rods and beams and 2-dimensional structures such as thin plates. For more complex

* Corresponding author. Tel.: +44 23 8059 4175; fax: +44 23 8059 3190.
*E-mail address:* brm@isvr.soton.ac.uk (B.R. Mace).

0022-460X/$ - see front matter © 2009 Elsevier Ltd. All rights reserved.
doi:10.1016/j.jsv.2009.06.005

structures or at higher frequencies the analysis becomes more difficult or even impossible, and the dispersion equation is often transcendental. Finding all the real, imaginary and complex solutions can be difficult and numerical solutions might be sought. Examples include layered media and laminated, fibre-reinforced, composite constructions or a smooth automotive tyre, which is homogeneous around the circumference. The equations of motion then become very complicated at best.

In such cases a numerical approach is very desirable. One approach, considered in this paper, is the wave and finite element (WFE) method, which combines conventional finite element analysis (FEA) with periodic structure theory. It is an attractive alternative to the spectral finite element method because conventional FEA methods, commercial packages and element libraries can be used, whereas in the latter approach special spectral elements must be developed on a case-by-case basis, which is not a trivial task.

The WFE method starts with FEA of a small segment of the structure. Since conventional FEA can be used for this modelling, existing element libraries and commercial FE packages can be fully utilised. The mass and stiffness matrices of the segment are found and post-processed by applying periodicity conditions for the propagation of a time-harmonic disturbance through the structure. Application of the periodicity conditions results in various eigenproblems whose solutions yield the dispersion relations for free wave propagation. These wave modes then form a basis from which forced response can be calculated.

There have been many applications of the WFE method. One difficulty is that numerical problems can occur. This is particularly true for 1-dimensional waveguides with complicated cross-sections, so that the size of the FE model of the small segment of the structure can be quite large. This paper concerns these numerical issues and describes ways to circumvent or reduce them. Attention is focused on the case of waveguides because numerical problems are generally far greater than for 2-dimensional structures.

For 1-dimensional structures there have been applications of the WFE method for free [3] and forced vibration [4], to rail structures [5] (and, in [6], using periodic structure theory for a track section), laminate plates [3], thin-walled structures [7] and fluid-filled [8,9] pipes. Mencik and Ichchou [10] applied the method to calculate wave transmission through a joint. There have been various applications to FEA of spatially periodic 1-dimensional structures. These include the earlier works of Orris and Petyt [11,12], Abdel-Rahman [13] and others reviewed by Mead in [14]. Specific applications include railway tracks [6], truss beams [15] and stiffened cylinders [16,17]. Other authors have applied periodic structure theory and FEA to 2-dimensional periodic structures, for example Ruzzene et al. [18], who considered periodic cellular cored structures. Mace and Manconi [19] applied the WFE method to 2-dimensional homogeneous solids and Manconi and Mace [20] extended the WFE approach to axisymmetric structures, including fluid-filled cylinders [21].

Various numerical issues occur in the application of the WFE method, but few papers describe them. One form of the eigenproblem involves forming the transfer matrix of the segment and determining its eigenvalues. This is very prone to ill-conditioning because there can be both very large and very small eigenvalues. Zhong and Williams [22] present the eigenvalue problem in a different form, exploiting the symplectic properties of the transfer matrix, and removing ill-conditioning problems in the eigenvalue problem. Various authors have considered FE discretisation effects and artefacts that arise because of the spatial discretisation of the structure (e.g. [3,4,23]). These artefacts are characteristic of wave propagation in periodic structures: spurious pass and stop bands and "aliasing" effects.

This paper concerns these and other numerical issues. First, free wave propagation is considered. In Section 2 the WFE approach is reviewed. The wavenumbers and wave modes are found by solving an eigenproblem. Various formulations for this eigenproblem are presented, the most appropriate formulation depending on the form of the solutions desired. In Section 3 various numerical issues are considered. These include FE discretisation errors and issues that arise from the spatial discretisation of the structure and consequent periodic structure artefacts—these issues arise if the size of the element is too large—and numerical truncation of inertia terms in the dynamic stiffness matrix, which occurs if the size of the element is too small. Concatenation of elements is proposed as a way of overcoming these difficulties. Numerical problems also arise because the eigenproblem may have both very large and very small eigenvalues. Zhong's method, and a method based on singular value decomposition, can be used to ameliorate these. The free waves form a basis on which the equations of motion can be projected. The basis can be reduced by retaining only the most important wave modes. A well-conditioned approach to forced response is described in Section 5. This exploits the orthogonality of the left and right eigenvectors. Numerical examples are presented. In Section 6 the results are summarised and concluding remarks made. Further details can be found in [24].

## 2. Free wave propagation and forms of the eigenvalue problem

In this section the WFE formulation for free wave propagation in a waveguide is reviewed. It begins with conventional FE analysis of only a short segment of the waveguide and application of periodicity conditions. The wavenumbers and wave mode shapes are found from the solution to an eigenproblem which can be posed in a number of ways. The most convenient form depends on the nature of the desired solutions, together with the numerical issues discussed in the next section.

### 2.1. Dynamic stiffness matrix and periodicity conditions

Consider a short of segment of length $\Delta$ of a waveguide as shown in Fig. 1. The waveguide is homogeneous along its axis $x$, but its properties can vary in an arbitrary manner over its cross-section. The segment is modelled using conventional FE methods. The equation of motion of the segment for time harmonic motion at angular frequency $\omega$ can be written as

$$\mathbf{D}\mathbf{q} = \mathbf{f}; \quad \mathbf{D} = \mathbf{K} + \mathrm{j}\omega\mathbf{C} - \omega^2\mathbf{M}, \tag{1}$$

where $\mathbf{D}$ is the dynamic stiffness matrix (DSM) and $\mathbf{K}$, $\mathbf{C}$ and $\mathbf{M}$ are the stiffness, viscous damping and mass matrices, respectively. The stiffness matrix may be complex if structural damping is present. Time harmonic motion of the form $\exp(\mathrm{j}\omega t)$ is implicit throughout this paper. The vectors

$$\mathbf{q} = \begin{Bmatrix} \mathbf{q}_L \\ \mathbf{q}_R \end{Bmatrix}; \quad \mathbf{f} = \begin{Bmatrix} \mathbf{f}_L \\ \mathbf{f}_R \end{Bmatrix} \tag{2}$$

contain the nodal degrees of freedom (DOFs) and forces, the subscripts $L$ and $R$ denoting the left and right sides of the segment, respectively. (Any internal DOFs can be condensed as described in Section 3.3.) Eq. (1) can be partitioned as

$$\begin{bmatrix} \mathbf{D}_{\mathrm{LL}} & \mathbf{D}_{\mathrm{LR}} \\ \mathbf{D}_{\mathrm{RL}} & \mathbf{D}_{\mathrm{RR}} \end{bmatrix} \begin{Bmatrix} \mathbf{q}_L \\ \mathbf{q}_R \end{Bmatrix} = \begin{Bmatrix} \mathbf{f}_L \\ \mathbf{f}_R \end{Bmatrix}. \tag{3}$$

The partitions are of size $n \times n$, where $n$ is the number of DOFs at the left-hand node of the segment. Since $\mathbf{D}$ is symmetric

$$\mathbf{D}_{\mathrm{LL}}^{\mathrm{T}} = \mathbf{D}_{\mathrm{LL}}, \quad \mathbf{D}_{\mathrm{RR}}^{\mathrm{T}} = \mathbf{D}_{\mathrm{RR}}, \quad \mathbf{D}_{\mathrm{LR}}^{\mathrm{T}} = \mathbf{D}_{\mathrm{RL}}, \tag{4}$$

where $(\cdot)^{\mathrm{T}}$ indicates the transpose.

Under the passage of a wave of the form $\exp \mathrm{j}(\omega t - kx)$ along the waveguide, Bloch's theorem [26] implies that the DOFs are related by the periodicity condition

$$\mathbf{q}_R = \lambda \mathbf{q}_L, \tag{5}$$

while equilibrium implies that

$$\lambda \mathbf{f}_L + \mathbf{f}_R = \mathbf{0}. \tag{6}$$

In these equations the propagation constant

$$\lambda = \mathrm{e}^{-\mathrm{j}k\Delta} \tag{7}$$

describes the amplitude and phase change over a distance $\Delta$ and $k$ is the wavenumber. The wavenumber can be purely real, purely imaginary or complex, associated with a propagating, a nearfield (evanescent) or an oscillating decaying wave, respectively.

### 2.2. Forms of the eigenvalue problem

The equations above lead to eigenvalue problems which can be posed in various ways. The solutions yield the eigenvalues $\lambda$, and hence WFE estimates of the wavenumber $k$, and the eigenvectors $\boldsymbol{\phi} = [\boldsymbol{\phi}_q^{\mathrm{T}} \ \boldsymbol{\phi}_f^{\mathrm{T}}]^{\mathrm{T}}$. These eigenvectors, or wave mode shapes, contain information concerning the DOFs and nodal forces under the passage of the wave through the partitions $\boldsymbol{\phi}_q$ and $\boldsymbol{\phi}_f$.

#### 2.2.1. The transfer matrix

The eigenproblem is often posed in terms of the transfer matrix $\mathbf{T}$ defined such that

$$\mathbf{T}\begin{Bmatrix} \mathbf{q}_L \\ \mathbf{f}_L \end{Bmatrix} = \lambda \begin{Bmatrix} \mathbf{q}_L \\ \mathbf{f}_L \end{Bmatrix}; \quad \mathbf{T} = \begin{bmatrix} -\mathbf{D}_{\mathrm{LR}}^{-1}\mathbf{D}_{\mathrm{LL}} & \mathbf{D}_{\mathrm{LR}}^{-1} \\ -\mathbf{D}_{\mathrm{RL}} + \mathbf{D}_{\mathrm{RR}}\mathbf{D}_{\mathrm{LR}}^{-1}\mathbf{D}_{\mathrm{LL}} & -\mathbf{D}_{\mathrm{RR}}\mathbf{D}_{\mathrm{LR}}^{-1} \end{bmatrix}. \tag{8}$$

The eigenvalues come in $n$ pairs $\lambda_i, 1/\lambda_i$ which represent a pair of positive- and negative-going waves. The eigenvalues and associated eigenvectors can be expressed as $(\lambda_i, \boldsymbol{\phi}_i^+)$ and $(1/\lambda_i, \boldsymbol{\phi}_i^-)$. Positive-going waves are those for which the magnitude of the eigenvalue is $<1$, i.e. $|\lambda_i|<1$, or, if $|\lambda_i| = 1$, the power is positive, i.e. $\mathrm{Re}\left\{\mathrm{j}\omega \boldsymbol{\phi}_{f,i}^{\mathrm{H}} \boldsymbol{\phi}_{q,i}\right\} < 0$ [3,4] where $(\cdot)^{\mathrm{H}}$ represents the

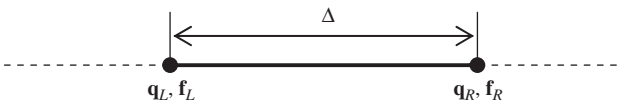


**Fig. 1.** A segment of a uniform waveguide.

complex conjugate transpose, or Hermitian. Alternatively the left eigenproblem

$$\boldsymbol{\psi}_i \mathbf{T} = \lambda_i \boldsymbol{\psi}_i \tag{9}$$

gives the same eigenvalues, while the orthogonality relations between the left and right eigenvectors can be expressed as

$$\boldsymbol{\psi}_i \boldsymbol{\phi}_j = d_i \delta_{ij}, \tag{10}$$

where $\delta_{ij}$ is the Kronecker delta and $d_i$ is arbitrary. Henceforth it is assumed that the eigenvectors are normalised such that $d_i = 1$.

Writing the eigenproblem in terms of the transfer matrix is convenient and, perhaps, intuitive. However, it is prone to poor numerical conditioning, especially for waveguides for which the FE model has a large number of DOFs. The eigenvalue problem (8) then contains both very small eigenvalues $\lambda$ and very large eigenvalues $1/\lambda$, representing waves that decay rapidly (by orders of magnitude perhaps) over the length $\Delta$ of the segment in the positive and negative $x$-directions, respectively. Furthermore $\mathbf{D}_{\mathrm{LR}}$ can be poorly conditioned so that determining its inverse is prone to numerical difficulties.

*2.2.2. The wave basis and model reduction*

The partitions of the left and right eigenvectors can be used to form the matrices

$$\boldsymbol{\Phi}_q^+ = [\boldsymbol{\phi}_{q,1}^+ \;\; \boldsymbol{\phi}_{q,2}^+ \;\; \cdots \;\; \boldsymbol{\phi}_{q,n}^+]; \quad \boldsymbol{\Psi}_q^+ = \begin{bmatrix} \boldsymbol{\psi}_{q,1}^+ \\ \boldsymbol{\psi}_{q,2}^+ \\ \\ \boldsymbol{\psi}_{q,n}^+ \end{bmatrix}. \tag{11}$$

Similar expressions hold for $\boldsymbol{\Phi}_q^-, \boldsymbol{\Psi}_q^-, \boldsymbol{\Phi}_f^\pm$, and $\boldsymbol{\Psi}_f^\pm$. These matrices, together with the orthogonality relations of Eq. (10), define transformations between the physical domain, in which the motion is described in terms of $\mathbf{q}$ and $\mathbf{f}$, and the wave domain, in which the motion is described in terms of waves of amplitudes $\mathbf{a}^+$ and $\mathbf{a}^-$ travelling in the positive and negative directions, respectively. Specifically,

$$\mathbf{q} = \boldsymbol{\Phi}_q^+ \mathbf{a}^+ + \boldsymbol{\Phi}_q^- \mathbf{a}^-; \quad \mathbf{f} = \boldsymbol{\Phi}_f^+ \mathbf{a}^+ + \boldsymbol{\Phi}_f^- \mathbf{a}^-. \tag{12}$$

In practice, as in modal analysis, only a number $m$ of the wave modes might be retained, so that the matrices $\boldsymbol{\Phi}_{q,f}^\pm$ and $\boldsymbol{\Psi}_{q,f}^\pm$ are $n \times m$ and $m \times n$, respectively. The number retained can be different at different frequencies. All propagating waves, for which $|\lambda| = 1$, must be retained together with the least-rapidly attenuating waves, e.g. for $|\lambda| < 1$, all those for which $|\lambda| > 0.1$, or some other user-defined criterion. For example, in Section 6 the retained wave modes are those for which $\mathrm{Im}\{k\Delta\} < 1$, i.e. $|\lambda| > \mathrm{e}^{-1}$. This is found to give acceptable accuracy. The reasons for reducing the size of the wave basis are partly that the size of the model is smaller, but primarily that the calculation of the high-order wave modes, which decay very rapidly with distance (by orders of magnitude over the element length), is very prone to poor numerical conditioning.

*2.2.3. Projection of the equations of motion onto the DOFs $\mathbf{q}_L$*

The equations of motion can be projected onto the DOFs $\mathbf{q}_L$ by pre-multiplying Eq. (3) by $[\lambda\mathbf{I} \;\; \mathbf{I}]$ and using Eqs. (5) and (6). It follows that:

$$[\lambda^2 \mathbf{D}_{\mathrm{LR}} + \lambda(\mathbf{D}_{\mathrm{LL}} + \mathbf{D}_{\mathrm{RR}}) + \mathbf{D}_{\mathrm{RL}}]\mathbf{q}_L = \mathbf{0}. \tag{13}$$

This quadratic eigenproblem for $\lambda$ can be written as the linear eigenproblem

$$\left[ \begin{bmatrix} \mathbf{0} & \mathbf{I} \\ -\mathbf{D}_{\mathrm{LR}}^{-1}\mathbf{D}_{\mathrm{RL}} & -\mathbf{D}_{\mathrm{LR}}^{-1}(\mathbf{D}_{\mathrm{LL}} + \mathbf{D}_{\mathrm{RR}}) \end{bmatrix} - \lambda \mathbf{I} \right] \begin{Bmatrix} \mathbf{q} \\ \lambda \mathbf{q} \end{Bmatrix} = 0. \tag{14}$$

Given the partition $\boldsymbol{\phi}_q$ of the resulting eigenvector, the eigenvector partition for the nodal forces is given by

$$\boldsymbol{\phi}_f = [\mathbf{D}_{\mathrm{LL}} + \lambda \mathbf{D}_{\mathrm{LR}}]\boldsymbol{\phi}_q. \tag{15}$$

This form of the eigenvalue problem is particularly useful for the analysis of free wave propagation in undamped waveguides (see Section 2.3).

*2.2.4. Zhong's method*

A third form of the eigenproblem is that due to Zhong et al. [22,27,28]. The method involves reformulating Eq. (3) in terms of the displacement vectors and application of the periodicity condition. The eigenvalue problem becomes

$$\begin{bmatrix} (\mathbf{D}_{\mathrm{LR}} - \mathbf{D}_{\mathrm{RL}}) & -(\mathbf{D}_{\mathrm{LL}} + \mathbf{D}_{\mathrm{RR}}) \\ (\mathbf{D}_{\mathrm{LL}} + \mathbf{D}_{\mathrm{RR}}) & (\mathbf{D}_{\mathrm{LR}} - \mathbf{D}_{\mathrm{RL}}) \end{bmatrix} \begin{Bmatrix} \mathbf{q} \\ \lambda \mathbf{q} \end{Bmatrix} = \frac{1}{(\lambda + 1/\lambda)} \begin{bmatrix} \mathbf{0} & \mathbf{D}_{\mathrm{LR}} \\ -\mathbf{D}_{\mathrm{RL}} & \mathbf{0} \end{bmatrix} \begin{Bmatrix} \mathbf{q} \\ \lambda \mathbf{q} \end{Bmatrix}. \tag{16}$$

Eq. (16) has repeated eigenvalues of $(\lambda + 1/\lambda)^{-1}$ since both $\lambda$ and $1/\lambda$ are solutions of Eq. (8). Note that the eigenvalues of most interest are those for which $|\lambda + 1/\lambda|^{-1}$ is largest. Corresponding to the repeated eigenvalues, there are two independent eigenvectors $\boldsymbol{\phi}_1'$ and $\boldsymbol{\phi}_2'$. The eigenvectors associated with the original eigenvalues $\lambda$ and $1/\lambda$ can be found

from a linear combination of $\boldsymbol{\phi}'_1$ and $\boldsymbol{\phi}'_2$ [22], i.e.:

$$\begin{Bmatrix} \boldsymbol{\phi}_q \\ \lambda\boldsymbol{\phi}_q \end{Bmatrix} = \alpha_1\boldsymbol{\phi}'_1 + \alpha_2\boldsymbol{\phi}'_2. \tag{17}$$

The eigenvectors $\boldsymbol{\phi}_f$ can once again be found from Eq. (15).

### 2.3. Desired solutions and the eigenproblem

The choice of the eigenproblem depends to an extent on the form of the solutions desired. For example, if it is desired to find the values of $\omega^2$ for a given propagation constant $\lambda$ then Eq. (13) can be rewritten as

$$[[\lambda^2\mathbf{K}_{\mathrm{LR}} + \lambda(\mathbf{K}_{\mathrm{LL}} + \mathbf{K}_{\mathrm{RR}}) + \mathbf{K}_{\mathrm{RL}}] - \omega^2[\lambda^2\mathbf{M}_{\mathrm{LR}} + \lambda(\mathbf{M}_{\mathrm{LL}} + \mathbf{M}_{\mathrm{RR}}) + \mathbf{M}_{\mathrm{RL}}]\mathbf{q}_L = 0. \tag{18}$$

This is a standard linear eigenproblem for $\omega^2$. This approach can be used to calculate the dispersion relations for free wave propagation in an undamped structure, since then real values of $k$ will lead to $n$ real solutions for $\omega$.

There are difficulties if the structure is damped since for a given real $\omega$ the eigenvalues $\lambda$ are complex, representing decaying waves with complex wavenumbers. There are also difficulties for general waveguides in finding solutions for complex wavenumbers. Under these circumstances either of the eigenproblems (8), (13) or (16) might be used, although (8) and (13) can suffer from numerical difficulties since there may be both very large and very small eigenvalues.

## 3. Numerical issues

Various numerical issues arise in the numerical calculation of free wave propagation characteristics using the WFE method and these affect the accuracy of WFE estimates. These issues, and methods to reduce their effects, are discussed in this section. The first two—FE discretisation errors and periodic structure artefacts—are relevant for all forms of the eigenproblem and occur in conventional applications of FEA. The last two—truncation of inertia terms in the DSM and numerical conditioning—are relevant only for the eigenproblems involving the DSM (Eqs. (8) and (16)).

### 3.1. Finite element discretisation and dispersion errors

At high frequencies FE discretisation errors become significant if the size of the element is too large [25]. As a rule-of-thumb, there should be at least six elements per wavelength, although the accuracy depends on the element shape function. Discretisation errors can be reduced by remeshing the structure using a shorter segment.

### 3.2. Spatial discretisation and periodic structure effects

The WFE model is a lumped, discrete, spring–mass structure which is spatially periodic with period $\Delta$ in the $x$ direction. At higher frequencies, when the segment length becomes comparable to the wavelength, periodic structure phenomena arise [14,26]. First, there is an aliasing effect: if $k\Delta$ is a solution to the eigenvalue problem then so, too, is $k\Delta + 2m\pi$ for any integer $m$, since they yield the same value for $\lambda$. Thus the wave modes and frequencies are periodic functions of the propagation constants. This is a well-known effect for periodic structures [26]. Secondly, periodic structures are known to exhibit a pass- and stop-band structure, in that disturbances can propagate freely only in certain frequency ranges, otherwise they decay with distance [14,29,30]. For a 1-dimensional element with $n$ DOFs per node there will be $n$ propagation bands. The bounds of these pass and stop bands are related to the natural frequencies of the periodic element under various boundary conditions [29,30].

In practical applications these are not important because the FE discretisation is known to be inaccurate for $k\Delta > 1$. The issue is one of determining which solutions to the eigenvalue problem are artifacts of the spatial discretisation and which are valid estimates of wavenumbers in the continuous structure. This can be achieved by determining the sensitivities of the estimated wavenumbers to the dimensions of the element, since the bounds of the pass and stop bands depend on the natural frequencies of the element with certain boundary conditions [29,30]. Thus increasing the size of the element both decreases the stiffness and increases the mass, hence reducing the bounding frequencies. Wavenumber estimates which are periodic artifacts are thus very sensitive to the dimensions of the element whereas those which provide estimates of wavenumbers in the continuum are insensitive to such changes.

Consider the solution for a given propagation constant $\lambda$ at frequency $\omega$. The sensitivity of the eigenvalue $\omega^2$ with respect to the segment length is [31]

$$\frac{\partial(\omega^2)}{\partial\Delta} = \boldsymbol{\phi}_j^{\mathrm{T}}\left[\frac{\partial\mathbf{K}}{\partial\Delta} - \omega^2\frac{\partial\mathbf{M}}{\partial\Delta}\right]\boldsymbol{\phi}_j. \tag{19}$$

This can be found analytically or by simple remeshing, and is often available in commercial packages. The sensitivity depends on the element type and shape function. The elements of the stiffness matrix $\mathbf{K}$ depend on $\Delta$ and decrease as $\Delta$ increases. They are proportional to $\Delta^{-n}$, where $n = 1$ for a linear shape function (e.g. a rod or a plane stress element) while

for higher order shape functions (e.g. cubic, describing bending in a thin beam) $n>1$. Similarly the elements of $\mathbf{M}$ increases as $\Delta$ increases and are proportional to $\Delta^{+m}$, where $m \geq 1$. Consequently the sensitivity is such that if

$$\frac{\Delta}{\omega^2}\frac{\partial(\omega^2)}{\partial\Delta} = O(1) \tag{20}$$

then the solution is a periodic artefact.

### 3.3. Round-off errors due to truncation of inertia terms in the DSM

Other numerical errors arise at very low frequencies when an eigenproblem based on the DSM is used. This occurs when $\mathbf{D}=\mathbf{K}-\omega^2\mathbf{M}$ is calculated numerically using finite precision arithmetic. If $K_{ij}$ is very large compared to $\omega^2 M_{ij}$ some digits associated with the inertia terms in $D_{ij}=K_{ij}-\omega^2 M_{ij}$ are truncated after the subtraction, leading to round-off errors and reduced numerical precision. The number of the digits truncated is approximately $n_{ij}=\log_{10}(|K_{ij}|/|\omega^2 M_{ij}|)$. Hence there is a frequency limit below which these numerical errors become unacceptably large.

These round-off errors could be reduced by remeshing with a longer segment. Alternatively higher precision arithmetic could be used. A more convenient and less costly approach is to retain the initial mesh (for which $\Delta$ is not large enough) and form a super-segment by concatenating a number of the original segments as shown in Fig. 2. The internal DOFs are then condensed. This method does not need re-modelling of a segment since the global stiffness and mass matrices can be formed from those of the original segment.

When no external forces are applied to the internal nodes the equation of motion of the concatenated segments can be written as

$$\begin{bmatrix} \tilde{\mathbf{D}}_{\mathrm{LL}} & \tilde{\mathbf{D}}_{\mathrm{LR}} & \tilde{\mathbf{D}}_{\mathrm{LI}} \\ \tilde{\mathbf{D}}_{\mathrm{RL}} & \tilde{\mathbf{D}}_{\mathrm{RR}} & \tilde{\mathbf{D}}_{\mathrm{RI}} \\ \tilde{\mathbf{D}}_{\mathrm{IL}} & \tilde{\mathbf{D}}_{\mathrm{IR}} & \tilde{\mathbf{D}}_{\mathrm{II}} \end{bmatrix} \begin{bmatrix} \mathbf{q}_L \\ \mathbf{q}_R \\ \mathbf{q}_I \end{bmatrix} = \begin{bmatrix} \mathbf{f}_L \\ \mathbf{f}_R \\ \mathbf{0} \end{bmatrix}, \tag{21}$$

where $\tilde{(\bullet)}$ denotes that the segment has internal nodes and is not condensed. The subscript $I$ indicates DOFs associated with the internal nodes. These can be removed using dynamic condensation [32] resulting in

$$\mathbf{D}\mathbf{q}_E = \mathbf{f}_E; \quad \mathbf{D} = [\tilde{\mathbf{D}}_{\mathrm{EE}} - \tilde{\mathbf{D}}_{\mathrm{EI}}\tilde{\mathbf{D}}_{\mathrm{II}}^{-1}\tilde{\mathbf{D}}_{\mathrm{IE}}], \tag{22}$$

where

$$\tilde{\mathbf{D}}_{\mathrm{EE}} = \begin{bmatrix} \tilde{\mathbf{D}}_{\mathrm{LL}} & \tilde{\mathbf{D}}_{\mathrm{LR}} \\ \tilde{\mathbf{D}}_{\mathrm{RL}} & \tilde{\mathbf{D}}_{\mathrm{RR}} \end{bmatrix}, \quad \tilde{\mathbf{D}}_{\mathrm{EI}} = \begin{bmatrix} \tilde{\mathbf{D}}_{\mathrm{LI}} \\ \tilde{\mathbf{D}}_{\mathrm{RI}} \end{bmatrix}, \quad \tilde{\mathbf{D}}_{\mathrm{IE}} = [\tilde{\mathbf{D}}_{\mathrm{IL}} \ \ \tilde{\mathbf{D}}_{\mathrm{IR}}], \quad \mathbf{q}_E = \begin{Bmatrix} \mathbf{q}_L \\ \mathbf{q}_R \end{Bmatrix}, \quad \mathbf{f}_E = \begin{Bmatrix} \mathbf{f}_L \\ \mathbf{f}_R \end{Bmatrix}. \tag{23}$$

Since the stiffness terms are reduced and the mass terms increased, errors due to truncation of inertia terms are consequently reduced.

While the internal DOFs may be dynamically condensed, computational cost increases because $\tilde{\mathbf{D}}_{\mathrm{II}}^{-1}$ must be evaluated at each frequency. Approximate expressions for the condensation can be developed and these reduce the computation cost. The inverse of the dynamic stiffness matrix associated with internal DOFs can be expressed as

$$\tilde{\mathbf{D}}_{\mathrm{II}}^{-1} = (\tilde{\mathbf{K}}_{\mathrm{II}} - \omega^2\tilde{\mathbf{M}}_{\mathrm{II}})^{-1} = (\mathbf{I} - \omega^2\tilde{\mathbf{K}}_{\mathrm{II}}^{-1}\tilde{\mathbf{M}}_{\mathrm{II}})^{-1}\tilde{\mathbf{K}}_{\mathrm{II}}^{-1}. \tag{24}$$

The first order approximation $\tilde{\mathbf{D}}_{\mathrm{II}}^{-1} \approx \tilde{\mathbf{K}}_{\mathrm{II}}^{-1}$ (i.e. static or Guyan reduction [16]) generally gives poor accuracy. However, Eq. (24) can be expanded in a power series in $\omega^2$ as

$$\tilde{\mathbf{D}}_{\mathrm{II}}^{-1} = (\mathbf{I} + \omega^2\tilde{\mathbf{K}}_{\mathrm{II}}^{-1}\tilde{\mathbf{M}}_{\mathrm{II}} + \omega^4\tilde{\mathbf{K}}_{\mathrm{II}}^{-1}\tilde{\mathbf{M}}_{\mathrm{II}}\tilde{\mathbf{K}}_{\mathrm{II}}^{-1}\tilde{\mathbf{M}}_{\mathrm{II}} + O\{(\omega^2\tilde{\mathbf{K}}_{\mathrm{II}}^{-1}\tilde{\mathbf{M}}_{\mathrm{II}})\}^3)\tilde{\mathbf{K}}_{\mathrm{II}}^{-1} \tag{25}$$

and after some manipulation it follows that:

$$\begin{aligned} \mathbf{D} \approx\ & (\tilde{\mathbf{K}}_{\mathrm{EE}} - \tilde{\mathbf{K}}_{\mathrm{EI}}\tilde{\mathbf{K}}_{\mathrm{II}}^{-1}\tilde{\mathbf{K}}_{\mathrm{IE}}) - \omega^2(\tilde{\mathbf{M}}_{\mathrm{EE}} - \tilde{\mathbf{K}}_{\mathrm{EI}}\tilde{\mathbf{K}}_{\mathrm{II}}^{-1}\tilde{\mathbf{M}}_{\mathrm{IE}} - \tilde{\mathbf{M}}_{\mathrm{EI}}\tilde{\mathbf{K}}_{\mathrm{II}}^{-1}\tilde{\mathbf{K}}_{\mathrm{IE}} + \tilde{\mathbf{K}}_{\mathrm{EI}}\tilde{\mathbf{K}}_{\mathrm{II}}^{-1}\tilde{\mathbf{M}}_{\mathrm{II}}\tilde{\mathbf{K}}_{\mathrm{II}}^{-1}\tilde{\mathbf{K}}_{\mathrm{IE}}) \\ & - \omega^4(\tilde{\mathbf{M}}_{\mathrm{EI}}\tilde{\mathbf{K}}_{\mathrm{II}}^{-1}\tilde{\mathbf{M}}_{\mathrm{IE}} - \tilde{\mathbf{K}}_{\mathrm{EI}}\tilde{\mathbf{K}}_{\mathrm{II}}^{-1}\tilde{\mathbf{M}}_{\mathrm{II}}\tilde{\mathbf{K}}_{\mathrm{II}}^{-1}\tilde{\mathbf{M}}_{\mathrm{IE}} - \tilde{\mathbf{M}}_{\mathrm{EI}}\tilde{\mathbf{K}}_{\mathrm{II}}^{-1}\tilde{\mathbf{M}}_{\mathrm{II}}\tilde{\mathbf{K}}_{\mathrm{II}}^{-1}\tilde{\mathbf{K}}_{\mathrm{IE}}). \end{aligned} \tag{26}$$

To calculate $\mathbf{D}$, $\tilde{\mathbf{K}}_{\mathrm{II}}^{-1}$ and the matrix expressions in parentheses need to be evaluated only once so that the computational cost is very small.

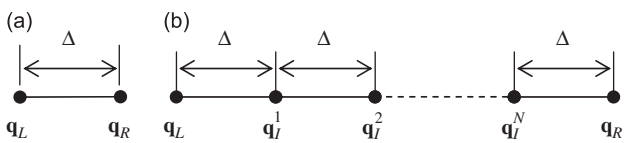


**Fig. 2.** (a) Single segment and (b) concatenated segments.

### 3.4. Numerical conditioning and eigenvectors

The eigenproblem of finding $\omega^2$ for given $\lambda$ (Eq. (18)) is a linear eigenproblem for which no special numerical conditioning issues arise. The eigenproblem of finding $\lambda$ for given $\omega^2$, on the other hand, can suffer from poor numerical conditioning, especially if the forms in Eqs. (8) and (13) are used, because there can be both very small eigenvalues $\lambda$ and very large eigenvalues $1/\lambda$.

The eigenproblem proposed by Zhong et al. (Eq. (16)) [22,27,28] does not suffer from these conditioning problems: the largest eigenvalues $(\lambda+1/\lambda)^{-1}$ are of interest. However, there can be numerical difficulties in determining the eigenvectors, especially at low frequencies when the eigenvectors of the wave modes are nearly parallel. These can be circumvented using an approach based on singular value decomposition (SVD).

The values of $\alpha_1$ and $\alpha_2$ in Eq. (17) may be calculated from (e.g. [4])

$$\begin{bmatrix} -\mathbf{D}_{\mathrm{RL}} & -\mathbf{D}_{\mathrm{LL}}-\mathbf{D}_{\mathrm{RR}}-\lambda\mathbf{D}_{\mathrm{LR}} \\ \lambda\mathbf{D}_{\mathrm{RL}} & -\mathbf{D}_{\mathrm{RL}} \end{bmatrix} \left\{ \alpha_1 \begin{Bmatrix} \mathbf{q}_1 \\ \lambda\mathbf{q}_1 \end{Bmatrix} + \alpha_2 \begin{Bmatrix} \mathbf{q}_2 \\ \lambda\mathbf{q}_2 \end{Bmatrix} \right\} = \mathbf{0}. \tag{27}$$

Premultiplication by $[\mathbf{q}_1^{\mathrm{H}} \;\; \lambda\mathbf{q}_1^{\mathrm{H}}]$ leads to the relationship

$$\frac{\alpha_2}{\alpha_1} = -\frac{[\mathbf{q}_1^{\mathrm{H}} \;\; \lambda\mathbf{q}_1^{\mathrm{H}}] \begin{bmatrix} -\mathbf{D}_{\mathrm{RL}} & -\mathbf{D}_{\mathrm{LL}}-\mathbf{D}_{\mathrm{RR}}-\lambda\mathbf{D}_{\mathrm{LR}} \\ \lambda\mathbf{D}_{\mathrm{RL}} & -\mathbf{D}_{\mathrm{RL}} \end{bmatrix} \begin{Bmatrix} \mathbf{q}_1 \\ \lambda\mathbf{q}_1 \end{Bmatrix}}{[\mathbf{q}_1^{\mathrm{H}} \;\; \lambda\mathbf{q}_1^{\mathrm{H}}] \begin{bmatrix} -\mathbf{D}_{\mathrm{RL}} & -\mathbf{D}_{\mathrm{LL}}-\mathbf{D}_{\mathrm{RR}}-\lambda\mathbf{D}_{\mathrm{LR}} \\ \lambda\mathbf{D}_{\mathrm{RL}} & -\mathbf{D}_{\mathrm{RL}} \end{bmatrix} \begin{Bmatrix} \mathbf{q}_2 \\ \lambda\mathbf{q}_2 \end{Bmatrix}}, \tag{28}$$

between $\alpha_1$ and $\alpha_2$. Although Eq. (28) is algebraically exact, there may be difficulties in accurate numerical calculation [24]. To avoid these, Eq. (27) can be written as

$$\mathbf{A} \begin{Bmatrix} \alpha_1 \\ \alpha_2 \end{Bmatrix} = \mathbf{0}; \quad \mathbf{A} = \begin{bmatrix} -\mathbf{D}_{\mathrm{RL}} & -\mathbf{D}_{\mathrm{LL}}-\mathbf{D}_{\mathrm{RR}}-\lambda\mathbf{D}_{\mathrm{LR}} \\ \lambda\mathbf{D}_{\mathrm{RL}} & -\mathbf{D}_{\mathrm{RL}} \end{bmatrix} \begin{bmatrix} \mathbf{q}_1 & \mathbf{q}_2 \\ \lambda\mathbf{q}_1 & \lambda\mathbf{q}_2 \end{bmatrix}, \tag{29}$$

with $\mathbf{A}$ being an $n\times 2$ rectangular matrix. The problem is equivalent to that of solving an overdetermined set of simultaneous equations if $n \geq 3$. Performing SVD on $\mathbf{A}$ gives $\mathbf{A} = \mathbf{U}\mathbf{S}\mathbf{V}^{\mathrm{H}}$, which can then be written as

$$\mathbf{A} \begin{bmatrix} v_{11} & v_{12} \\ v_{21} & v_{22} \end{bmatrix} = \mathbf{U} \begin{bmatrix} \sigma_1 & 0 & 0 & \cdots & 0 \\ 0 & \sigma_2 & 0 & \cdots & 0 \end{bmatrix}^{\mathrm{T}}, \tag{30}$$

where $\sigma_2 \approx 0$. Taking the second column of Eq. (30) gives

$$\mathbf{A} \begin{Bmatrix} v_{12} \\ v_{22} \end{Bmatrix} \approx \mathbf{0} \tag{31}$$

and hence $\alpha_1$ and $\alpha_2$ are such that

$$\frac{\alpha_2}{\alpha_1} = \frac{v_{22}}{v_{12}}. \tag{32}$$

This ratio can be evaluated directly from Eq. (31).

## 4. Free wave propagation: numerical examples

In this section the computational issues are illustrated with two examples for which analytical solutions are known.

### 4.1. Free wave propagation in a Euler–Bernoulli beam

For a Euler–Bernoulli beam there is a pair of propagating and a pair of nearfield waves (e.g. [1]) with wavenumbers given by

$$k = \pm k_B, \mathrm{j}k_B, \tag{33}$$

where $k_B = \sqrt[4]{\rho A\omega^2/EI}$ is the bending wavenumber of the beam. Here $EI$ is the bending stiffness, $\rho$ is the mass density and $A$ the cross-sectional area. Denoting the propagating and nearfield waves with the subscripts $p$ and $n$ the wave modes are [1]

$$\boldsymbol{\phi}_p^{\pm} = \begin{Bmatrix} w \\ \theta \\ V \\ M \end{Bmatrix} = \begin{Bmatrix} 1 \\ \mp\mathrm{j}k_B \\ \mp\mathrm{j}EIk_B^3 \\ -EIk_B^2 \end{Bmatrix}; \quad \boldsymbol{\phi}_n^{\pm} = \begin{Bmatrix} 1 \\ \mp k_B \\ \pm EIk_B^3 \\ EIk_B^2 \end{Bmatrix}, \tag{34}$$

where the subscript $\pm$ indicates the direction of propagation or attenuation. Here $w$ is the translational displacement, $\theta = \partial w/\partial x$ is the rotation, $M = EI\partial^2 w/\partial x^2$ is the bending moment and $V = -EI\partial^3 w/\partial x^3$ is the shear force.

A 2-noded element of length $\Delta$, with 2 DOFs per node $(w, \theta)$, is taken. Assuming a cubic polynomial shape function, the mass and stiffness matrices are [25]

$$\mathbf{K} = \frac{EI}{\Delta^3}\begin{bmatrix} 12 & 6\Delta & -12 & 6\Delta \\ & 4\Delta^2 & -6\Delta & 2\Delta^2 \\ \text{sym.} & & 12 & -6\Delta \\ & & & 4\Delta^2 \end{bmatrix}, \quad \mathbf{M} = \frac{\rho A\Delta}{420}\begin{bmatrix} 156 & 22\Delta & 54 & -13\Delta \\ & 4\Delta^2 & 13\Delta & -3\Delta^2 \\ \text{sym.} & & 156 & -22\Delta \\ & & & 4\Delta^2 \end{bmatrix}. \tag{35}$$

The eigenvalues and eigenvectors follow straightforwardly (e.g. [24]). The wavenumbers are given by

$$k_{1,2} = k_B(\pm 1 \mp (k_B\Delta)^4/2880 - \mathrm{j}(k_B\Delta)^5/2880\ldots),$$

$$k_{3,4} = -\mathrm{j}k_B(\pm 1 \mp (k_B\Delta)^4/2880 - \mathrm{j}(k_B\Delta)^5/2880\ldots), \tag{36}$$

where the wavenumbers $k_{1,2}$ are related to the propagating waves while $k_{3,4}$ are related to the nearfield waves. The relative errors in the wavenumbers are $O\{(k_B\Delta)^4\}$. The eigenvectors associated with $k_{1,2}$ are

$$\boldsymbol{\Phi}_p^{\pm} = \begin{Bmatrix} 1 \\ \mp\mathrm{j}k_B(1 \mp (k_B\Delta)^4/2880 \pm (k_B\Delta)^6/10\,800\ldots) \\ \mp\mathrm{j}EIk_B^3(1 \mp (k_B\Delta)^4/960 \mp 13(k_B\Delta)^6/302\,400\ldots) \\ -EIk_B^2(1 - (k_B\Delta)^4/1440 - (k_B\Delta)^6/18\,900\ldots) \end{Bmatrix}. \tag{37}$$

The errors in the elements of the eigenvectors (37) are $O\{(k_B\Delta)^4\}$ relative to the analytical solution. Similar expressions hold for $k_{3,4}$ with the relative errors again being $O\{(k_B\Delta)^4\}$.

Numerical results are now calculated using the element matrices (35). All the calculations were performed using MATLAB 7.0.4 and double precision arithmetic was used so that numbers are accurate to 16 digits. The relative error in the predicted propagating wavenumber, $|(k - k_B)/k_B|$, is shown in Fig. 3. The relative error in the rotational DOF per unit displacement is shown for the positive-going propagating wave in Fig. 4. In both figures the relative errors are minimum at around $k_B\Delta = 0.04$. Above and below $k_B\Delta = 0.04$ the relative errors increase. Above $k_B\Delta = 0.04$, the relative errors increase due to FE discretisation errors (Section 3.1). For the Euler–Bernoulli beam the error increases at a rate proportional to $(k_B\Delta)^4$, see Eqs. (36) and (37).

Below $k_B\Delta = 0.04$ the relative errors increase as $k_B\Delta$ decreases. This is due to round-off errors introduced by truncation of inertia terms when $\mathbf{D} = \mathbf{K} - \omega^2\mathbf{M}$ is evaluated. For the diagonal elements of the matrices the number of digits lost is approximately

$$n_{ii} = \log_{10}(K_{ii}/\omega^2 M_{ii}) \tag{38}$$

and if $n_{ii} = 16$ then, if double precision calculations are used, all information concerning the mass matrix is lost. For the Euler–Bernoulli beam the element matrices are given in Eq. (35) and $\max\{K_{ii}/\omega^2 M_{ii}\} = 420/(k_B\Delta)^4$ for $i = 2, 4$. The asymptote of the relative error for small $k_B\Delta$ is thus proportional to $(k_B\Delta)^{-4}$. As can be seen in Figs. 3 and 4, the inertia terms are completely rounded-off if $k_B\Delta < 4 \times 10^{-4}$ or so.

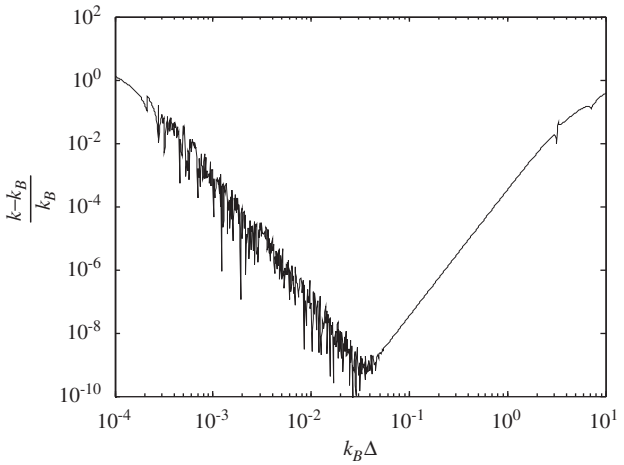


**Fig. 3.** Relative error in the propagating wavenumber of a thin beam.

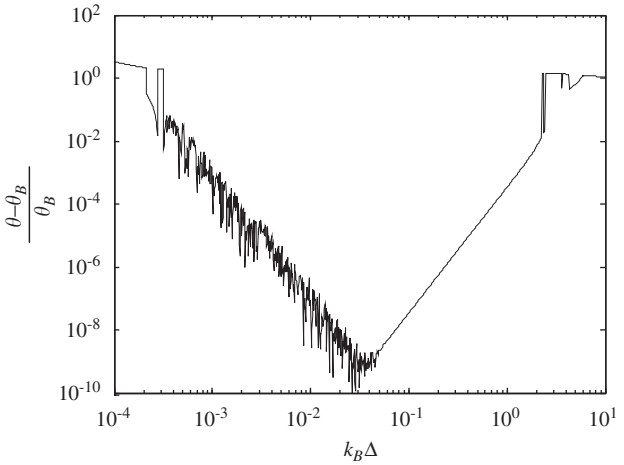


**Fig. 4.** Relative error in $\theta_B$ of a thin beam.

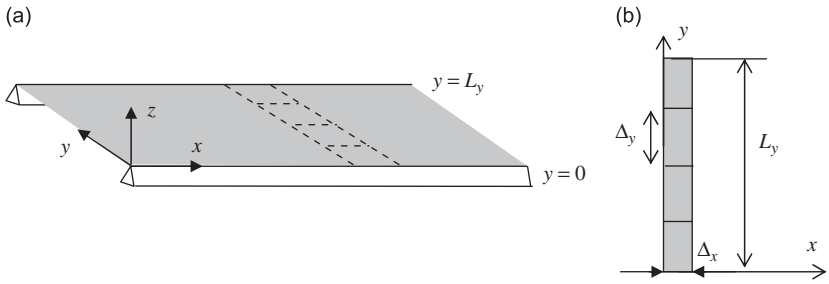


**Fig. 5.** (a) Plate strip with simply supported boundaries and (b) four element model.

### 4.2. Free wave propagation in a thin plate strip

Consider free flexural wave propagation in a plate strip as shown in Fig. 5. The plate is thin, isotropic, undamped and of width $L_y$, and the $y$-wise plate edges are simply supported. For such a plate strip, the wave modes have displacements proportional to $\sin(i\pi y/L_y)$. The wavenumber is then (e.g. [1])

$$k_{xi}^2 = \pm\sqrt{\frac{\rho h}{D}}\omega - \left(\frac{i\pi}{L_y}\right)^2 \quad (i = 1, 2, \ldots), \tag{39}$$

where $D = Eh^3/12(1-\nu^2)$ is the bending rigidity, $h$ is the thickness of the plate strip and $\nu$ is Poisson's ratio.

The plate is assumed to be steel with $L_y = 0.18$, $E = 2.0 \times 10^{11}$, $\rho = 7800$, $\nu = 0.30$ and $h = 1.8 \times 10^{-3}$, all in SI units. A segment of width $\Delta_x$ in the $x$-direction is taken across the width of the strip and meshed using rectangular elements of dimension $\Delta_x \times \Delta_y$. Fig. 5(b) shows an example using four elements. The mass and stiffness matrices were formed using ANSYS 7.1. The four node shell element SHELL63 was chosen. Subsequent processing was performed in Matlab 7.0.4 using double precision arithmetic.

Consider first the model with just four elements across the strip (Fig. 5(b)) with $\Delta_x = 18\,\text{mm}$, $\Delta_y = 45\,\text{mm}$. After removal of the in-plane DOFs there are 22 DOFs in the WFE model. The dispersion curves for the $i = 1$ mode are shown in Fig. 6. There are two waves: one is a wave which propagates above its cut-off frequency and the other is a nearfield wave. Figs. 6(a) and (b) show the dispersion curves calculated from the eigenvalue problem using the transfer matrix (8) and Zhong's method (Eq. (16)), respectively. The abscissa is the non-dimensional frequency

$$\Omega = \frac{L_y^2}{\pi^2}\sqrt{\frac{\rho h}{D}}\omega. \tag{40}$$

The cut-off frequency for the $i$th mode occurs at $\Omega = i^2$. The ordinate shows the non-dimensional wavenumber, $k_x L_y/\pi$, which equals $-ji$ for the $i$th wave mode at $\Omega = 0$. It can be seen that the results using the transfer matrix (Fig. 6(a)) are very inaccurate around the cut-off frequency. This is a typical example of deterioration due to the ill-conditioning of the eigenvalue problem. For the plate strip, the condition number of the eigenvalue problem using the transfer matrix is $O(10^{13})$ while that using Zhong's method is $O(10^5)$. For a larger matrix (with more DOFs), results using the transfer matrix

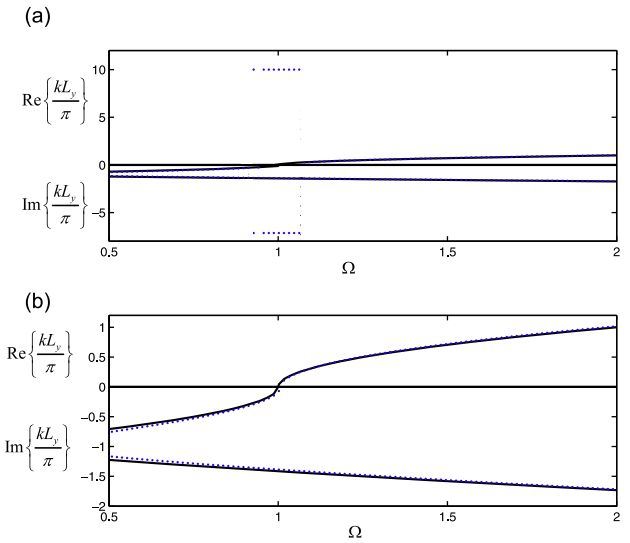


**Fig. 6.** Flexural waves in a plate strip with simply supported edges. Dispersion curves: — analytical solution; ⋯ the WFE result using (a) the transfer matrix approach and (b) Zhong's method.

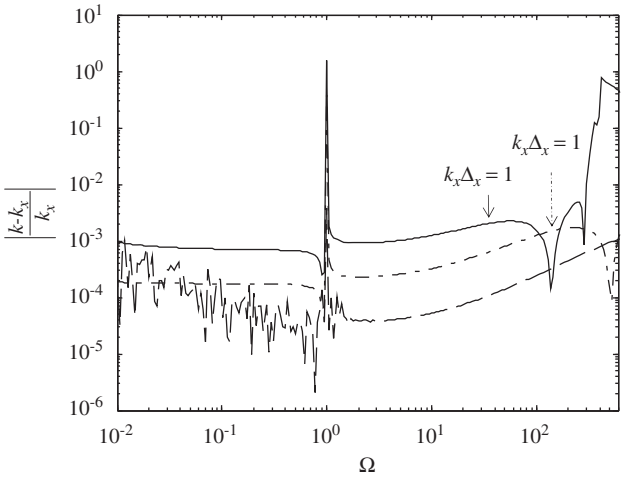


**Fig. 7.** Relative error in the wavenumber for the $i = 1$ wave mode: — 18; – · – 36; and – – 90 element plate strip model. Frequencies where $k_x\Delta_x = 1$ are marked for 18 and 36 element models.

can completely break down. Further examples can be found in [24]. The errors in Fig. 6(b) as $\Omega \to 0$ are due to the coarse FE discretisation.

Hereafter only results using Zhong's method are shown. Fig. 7 shows the relative errors in the propagating wavenumber of the $i = 1$ wave mode for models with various numbers of square elements across the plate strip. Three models are considered: 18 elements ($\Delta_x = \Delta_y = 10$ mm), 36 elements ($\Delta_x = \Delta_y = 5$ mm) and 90 elements ($\Delta_x = \Delta_y = 2$ mm). For the 90 element model $k_x\Delta_x = 1$ around $\Omega = 900$. For the other models the frequency where $k_x\Delta_x = 1$ is indicated. At the cut-off frequency ($\Omega = 1$) the wavenumber $k_{x1} = 0$ and hence the relative errors can be very large. The FE discretisation errors become smaller for the FE models with smaller values of $\Delta_x$ and $\Delta_y$. However, the round-off errors due to truncation of inertia terms increase at low frequencies for the 90 element model, for which $\Delta_x$ is smallest.

The relative error in the calculated shear force per unit translational displacement $V_{xz}/w$ is shown in Fig. 8. The eigenvector is evaluated using the SVD approach described in Section 3.4. The analytical expression for the shear force is [1]

$$V_{xz}/w = \mathrm{j}Dk_x(k_x^2 + (2 - \nu)k_y^2). \tag{41}$$

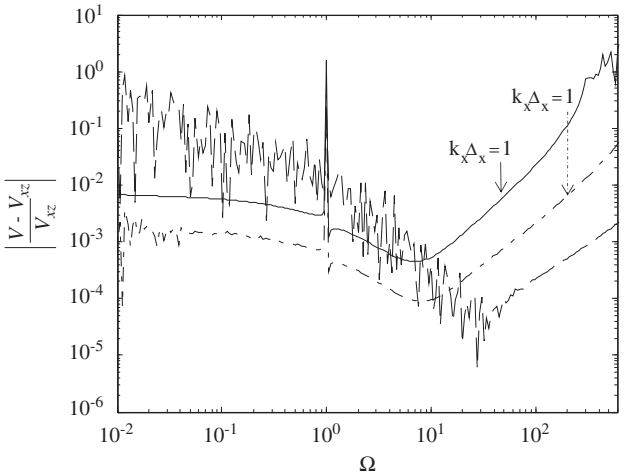


**Fig. 8.** Relative errors in $V_{xz}/w$ for the plate strip with simply supported edges. Notation is same as Fig. 7.

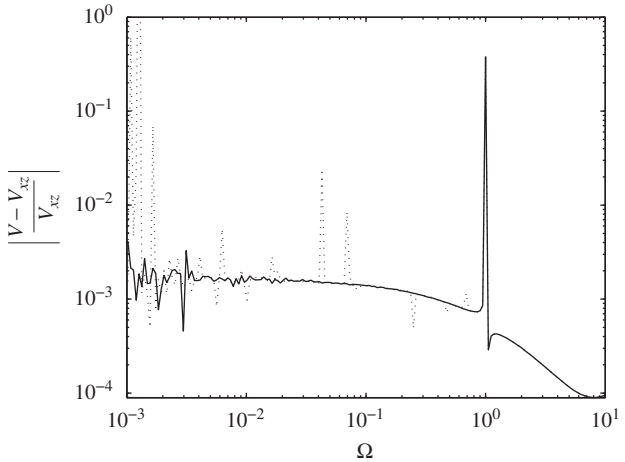


**Fig. 9.** Relative errors in $\tau_{xz}/w$ for the plate strip with simply supported edges: · · · · · direct solution for eigenvectors and — eigenvectors found using SVD.

The relative errors associated with the 18 and 36 element models are similar to, but somewhat larger than, those for the wavenumber. At higher frequencies the errors are due to discretisation and decrease as the size of the elements decreases. However, the error associated with the 90 element model is very large at lower frequencies because $k_x\Delta_x$ is small, the matrix size is large and the effects of round-off errors are substantial.

Fig. 9 shows the relative error in the shear force per unit translational displacement $V_{xz}/w$ for the model with 36 elements and with the eigenvector evaluated directly (Eq. (28)) and using SVD (Eq. (32)). It can be seen that the direct solution is prone to very large errors, especially at low frequencies.

Fig. 10 shows the relative errors in $V_{xz}/w$ using the original 90 element model ($\Delta_x = \Delta_y = 2$ mm) and the concatenated model (two segments, each $\Delta_x = \Delta_y = 2$ mm). The error using 90 rectangular elements ($\Delta_x = 4$ mm, $\Delta_y = 2$ mm) is also shown—this modelled region has the same dimensions as the concatenated model. For the models with 2 mm long elements it can be seen that concatenating two segments significantly reduces numerical errors at low frequencies. The errors for the model with 4 mm long elements are larger than those for the concatenated model, with dispersion errors being noticeable at high frequencies. Furthermore, this also requires remeshing. Finally Fig. 11 shows the relative errors in the concatenated model using dynamic condensation and the second order expansion of Eq. (26). Differences are only significant at high frequencies.

## 5. Forced response using a wave approach

The forced response of a waveguide can be calculated in terms of waves, usually by projecting the equations of motion onto the wave basis defined in Eq. (12). Four steps are typically involved: determining the amplitudes of the waves in an

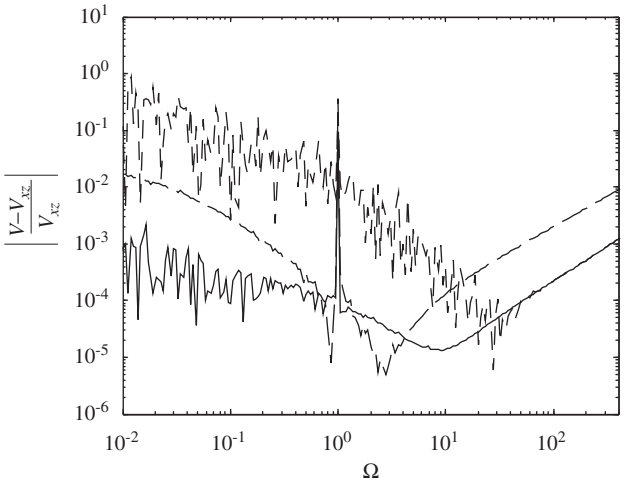


**Fig. 10.** Relative errors in $V_{xz}/w$ for the plate strip with simply supported edges: · · · · · the FE model with 90 elements; — the concatenated model; and – – rectangular element model.

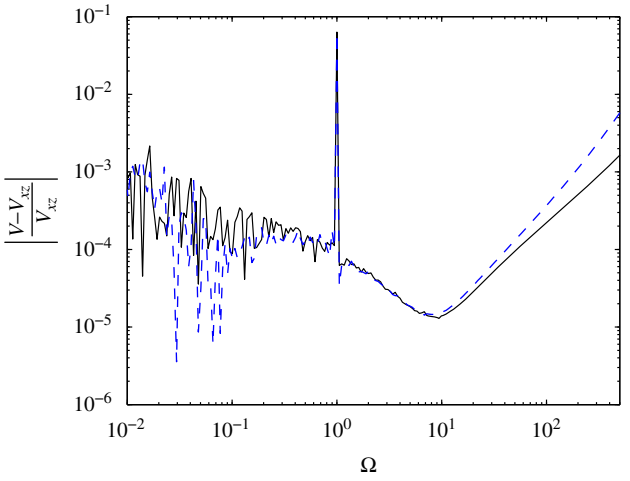


**Fig. 11.** Relative errors in $\tau_{xz}/w$ for the plate strip with simply supported edges: — dynamic condensation and – – the second order approximation.

infinite waveguide that are excited by point excitation; calculation of the reflection matrices for boundaries (and also perhaps other discontinuities); assembling the system equations involving excitation, reflection and propagation; solution of the equations and determining the physical response by superimposing wave amplitudes at a response point. The procedure is described in detail in, for example, [34–37]. Here the numerical issues associated with the procedure are discussed. These primarily concern ill-conditioning, and care should be taken to formulate the problem so that it is well-conditioned. This normally involves using a reduced wave basis and exploiting the orthogonality of the left and right eigenvectors as described in Section 2.2.1.

### 5.1. Determining the amplitudes of directly excited waves

External forces applied to an infinite waveguide generate waves whose amplitudes are given by the vectors $\mathbf{e}^{+}$ and $\mathbf{e}^{-}$ which propagate outwards from the excitation point in the positive and negative $x$-directions, respectively. Continuity and equilibrium equations can be written at the excitation point. These can be projected onto the wave basis using equation (12) to give

$$\begin{bmatrix} \boldsymbol{\Phi}_q^{+} & -\boldsymbol{\Phi}_q^{-} \\ \boldsymbol{\Phi}_f^{+} & -\boldsymbol{\Phi}_f^{+} \end{bmatrix} \begin{Bmatrix} \mathbf{e}^{+} \\ \mathbf{e}^{-} \end{Bmatrix} = \begin{Bmatrix} \mathbf{0} \\ \mathbf{f}_{\text{ext}} \end{Bmatrix}, \tag{42}$$

where $\mathbf{f}_{\text{ext}}$ is the vector of external forces. If all $n$ wave modes are retained then, in principle, the excited wave amplitudes may be directly determined from Eq. (42) as

$$\begin{Bmatrix} \mathbf{e}^+ \\ \mathbf{e}^- \end{Bmatrix} = \begin{bmatrix} \mathbf{\Phi}_q^+ & -\mathbf{\Phi}_q^- \\ \mathbf{\Phi}_f^+ & -\mathbf{\Phi}_f^+ \end{bmatrix}^{-1} \begin{Bmatrix} \mathbf{0} \\ \mathbf{f}_{\text{ext}} \end{Bmatrix}. \tag{43}$$

However, numerical problems are likely to occur, especially for complicated structures, because the matrix being inverted can be ill-conditioned.

First, numerical problems are most evident for the highest order wave modes, i.e. those that decay most rapidly with distance. These are of little interest as far as the forced response is concerned, however. In practice, therefore, only the first $m$ wave modes might be retained, these being the $m$ wave modes for which $|\text{Im}(k)|$ is smallest. The matrix in Eq. (42) is then no longer square. A pseudo-inverse could be calculated or singular value decomposition used.

Alternatively, the orthogonality of the left and right eigenvectors of the transfer matrix, i.e. Eq. (10), can be exploited. Premultiplying Eq. (42) by the matrix of left eigenvectors $\mathbf{\Psi} = [\mathbf{\Psi}^{+\text{T}} \ \ \mathbf{\Psi}^{-\text{T}}]^{\text{T}}$ gives

$$\begin{bmatrix} \mathbf{\Psi}_f^+ & \mathbf{\Psi}_q^+ \\ \mathbf{\Psi}_f^- & \mathbf{\Psi}_q^- \end{bmatrix} \begin{bmatrix} \mathbf{\Phi}_q^+ & -\mathbf{\Phi}_q^- \\ \mathbf{\Phi}_f^+ & -\mathbf{\Phi}_f^- \end{bmatrix} \begin{Bmatrix} \mathbf{e}^+ \\ \mathbf{e}^- \end{Bmatrix} = \begin{bmatrix} \mathbf{\Psi}_f^+ & \mathbf{\Psi}_q^+ \\ \mathbf{\Psi}_f^- & \mathbf{\Psi}_q^- \end{bmatrix} \begin{Bmatrix} \mathbf{0} \\ \mathbf{f}_{\text{ext}} \end{Bmatrix}. \tag{44}$$

Noting the orthogonality conditions $\mathbf{\Psi}^{\pm}\mathbf{\Phi}^{\pm} = \mathbf{I}$, $\mathbf{\Psi}^{\pm}\mathbf{\Phi}^{\mp} = \mathbf{0}$, it follows that:

$$\begin{Bmatrix} \mathbf{e}^+ \\ \mathbf{e}^- \end{Bmatrix} = \begin{Bmatrix} \mathbf{\Psi}_q^+\mathbf{f}_{\text{ext}} \\ -\mathbf{\Psi}_q^-\mathbf{f}_{\text{ext}} \end{Bmatrix}. \tag{45}$$

Eq. (45) is always well-conditioned.

### 5.2. Reflection coefficient matrix

Waves $\mathbf{a}^+$ incident on a boundary give rise to reflected waves $\mathbf{a}^-$ such that

$$\mathbf{a}^- = \mathbf{R}\mathbf{a}^+, \tag{46}$$

where $\mathbf{R}$ is a matrix of reflection coefficients. The boundary conditions can always be written in the form

$$\mathbf{A}\mathbf{f} + \mathbf{B}\mathbf{q} = \mathbf{0} \tag{47}$$

where $\mathbf{f}$ and $\mathbf{q}$ are the forces and DOFs at the boundary and where $\mathbf{A}$ and $\mathbf{B}$ are matrices whose elements are in general complex and frequency dependent. In many cases Eq. (47) can be written in terms of a dynamic stiffness matrix (if $\mathbf{A}$ is invertible) while simple expressions exist for some commonly assumed boundary conditions (e.g. for a fixed boundary $\mathbf{A} = \mathbf{0}$ and $\mathbf{B} = \mathbf{I}$, while for a force-free boundary $\mathbf{B} = \mathbf{0}$ and $\mathbf{A} = \mathbf{I}$). The displacement and force vectors in Eq. (47) are again expressed in terms of waves so that the reflection coefficient matrix becomes

$$\mathbf{R} = -(\mathbf{A}\mathbf{\Phi}_f^- + \mathbf{B}\mathbf{\Phi}_q^-)^{-1}(\mathbf{A}\mathbf{\Phi}_f^+ + \mathbf{B}\mathbf{\Phi}_q^+). \tag{48}$$

Again there are possible numerical difficulties. If only $m<n$ wave modes are retained then a pseudo-inverse can be used to estimate $\mathbf{R}$, while orthogonality between left and right eigenvectors can again be exploited. For example, for fixed and free boundaries the reflection matrices are

$$\mathbf{R}_{\text{fixed}} = -\mathbf{\Psi}_f^-\mathbf{\Phi}_q^+; \quad \mathbf{R}_{\text{free}} = -\mathbf{\Psi}_q^-\mathbf{\Phi}_f^+. \tag{49}$$

Again, these are always well-conditioned. Similar expressions exist for waves $\mathbf{a}^-$ incident on a left-hand boundary.

### 5.3. Assembly, solution and response determination

Once the wave amplitudes $\mathbf{a}^+$ and $\mathbf{a}^-$ at a location are known, the DOFs and internal forces follow from Eq. (12). The wave amplitudes can be determined by considering the excitation and reflection relations described above together with wave propagation relations. The procedure is outlined in more detail in [35,36], while the application of the WFE method to the analysis of the forced vibration of a tyre is considered in [33].

As a simple example, consider the finite waveguide shown in Fig. 12 excited at the point $x_e$. The wave amplitudes $\mathbf{a}^+$ and $\mathbf{g}^-$ at the excitation point are the sum of the directly excited waves $\mathbf{e}^+$ and $\mathbf{e}^-$ and the incident waves $\mathbf{g}^+$ and $\mathbf{a}^-$, hence

$$\mathbf{a}^+ = \mathbf{e}^+ + \mathbf{g}^+, \quad \mathbf{g}^- = \mathbf{e}^- + \mathbf{a}^-. \tag{50}$$

Propagation and reflection relations such as

$$\mathbf{c}^+ = \mathbf{T}(L - x_e)\mathbf{a}^+; \quad \mathbf{a}^- = \mathbf{T}(L - x_e)\mathbf{c}^-; \quad \mathbf{d}^+ = \mathbf{R}_L\mathbf{d}^-; \quad \mathbf{c}^- = \mathbf{R}_R\mathbf{c}^+ \tag{51}$$

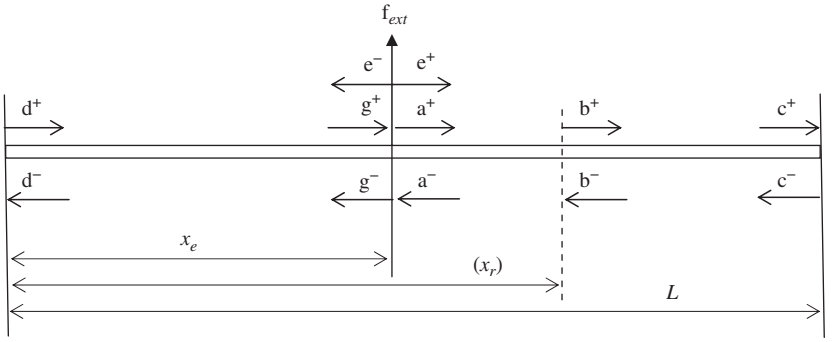


**Fig. 12.** Wave amplitudes in a finite structure.

can be written, where $\mathbf{R}_L$ and $\mathbf{R}_R$ are the reflection matrices at the left and right ends of the waveguide and

$$\mathbf{T}(x) = \mathrm{diag}(\mathrm{e}^{-\mathrm{j}k_1 x}, \mathrm{e}^{-\mathrm{j}k_2 x}, \ldots, \mathrm{e}^{-\mathrm{j}k_m x}) \tag{52}$$

is the wave propagation matrix $\mathbf{T}$ that relates the wave amplitudes at two points a distance $x$ apart. Using this formulation, the magnitudes of the elements of $\mathbf{T}$ are all $\leq 1$, with the elements corresponding to the high order wave modes being approximately zero. This ensures good numerical conditioning.

Using the above relations, $\mathbf{a}^+$ in Eq. (50) can be expressed, after some manipulation, as

$$\mathbf{a}^+ = \mathbf{e}^+ + \mathbf{T}(x_e)\mathbf{R}_L\mathbf{T}(L)\mathbf{R}_R\mathbf{T}(L-x_e)\mathbf{a}^+ + \mathbf{T}(x_e)\mathbf{R}_L\mathbf{T}(x_e)\mathbf{e}^-, \tag{53}$$

and hence

$$\mathbf{a}^+ = \{\mathbf{I} - \mathbf{T}(x_e)\mathbf{R}_L\mathbf{T}(L)\mathbf{R}_R\mathbf{T}(L-x_e)\}^{-1}\{\mathbf{e}^+ + \mathbf{T}(x_e)\mathbf{R}_L\mathbf{T}(x_e)\mathbf{e}^-\}, \tag{54}$$

where $L$ is the total length of the waveguide. In a similar manner the negative going waves

$$\mathbf{a}^- = \{\mathbf{I} - \mathbf{T}(L-x_e)\mathbf{R}_R\mathbf{T}(L)\mathbf{R}_L\mathbf{T}(x_e)\}^{-1}\{\mathbf{e}^- + \mathbf{T}(L-x_e)\mathbf{R}_R\mathbf{T}(L-x_e)\mathbf{e}^+\} - \mathbf{e}^-. \tag{55}$$

The wave amplitudes at some response point $x_r$ are

$$\mathbf{b}^+ = \mathbf{T}(x_r - x_e)\mathbf{a}^+; \quad \mathbf{b}^- = \mathbf{T}(L-x_r)\mathbf{R}_R\mathbf{T}(L-x_r)\mathbf{b}^+, \tag{56}$$

and the total response at the excitation and response points can be obtained by substituting the expressions for the wave amplitudes into Eq. (12). The above solution is always well-conditioned because the matrices being inverted are diagonally dominant, the elements of $\mathbf{T}$ all being $\leq 1$.

## 6. Illustrative example of a plate

The forced response of the thin, rectangular plate shown in Fig. 13 is considered. The plate is assumed to be steel ($E = 2.0 \times 10^{11}$, $\rho = 7800$, $\nu = 0.3$) with $L_x = 0.6$, $L_y = 0.18$ and the thickness $h = 0.0018$, all in SI units. All edges are simply supported. The locations where the point excitation is applied and the response is calculated are $(x_e, y_e)$ and $(x_r, y_r)$, respectively. A loss factor $\eta = 0.03$ is assumed. The wavenumbers and wave modes then become complex.

The response as a sum of modes is [2]

$$w(x_r, y_r) = \frac{4f_{\mathrm{ext}}}{\rho h L_x L_y} \sum_{m=1}^{\infty}\sum_{n=1}^{\infty} \frac{\phi_{mn}(x_r, y_r)\phi_{mn}(x_e, y_e)}{\{\omega_{mn}^2(1+\mathrm{j}\eta) - \omega^2\}}, \tag{57}$$

where $\phi_{mn}(x,y) = \sin(m\pi x/L_x)\sin(n\pi y/L_y)$ and $\omega_{mn} = \pi^2\sqrt{D/\rho h}\{(m/L_x)^2 + (n/L_y)^2\}$. In the numerical examples 1000 modes were taken. For the WFE calculations the plate strip model of Section 4.2, with 36 elements across the cross-section ($\Delta_x = \Delta_y = 5$ mm), was used. The reflection matrices for simply supported boundaries are $\mathbf{R}_{L,R} = -\mathbf{I}$.

Fig. 14 shows the magnitude of the input mobility. The non-dimensional frequency $\Omega$ is defined in Eq. (40). Since the model has 214 DOFs, 214 wave modes can be obtained at each frequency. However, in Fig. 14 a reduced number of wave modes is used, only the waves associated with $\mathrm{Im}\{k\Delta\} < 1$ being retained for the WFE result. In the frequency range shown, only about 17 positive- and negative-going pairs of wave modes are retained, these being all the propagating waves and some of the nearfield waves. Furthermore the excited wave amplitudes are calculated using the well-conditioned approach leading to Eq. (45). Good agreement can be seen. This implies that the contribution of the strongly decaying waves to the forced response is negligible—they are extremely stiff and difficult to excite. If the transfer response is of concern, nearfield waves are even less significant and only a few nearfield waves are important [24].

If instead all the wave modes are included, the calculated result breaks down as shown in Fig. 15. This is because of the poor numerical conditioning associated with the highest order wave modes, which are the very rapidly decaying waves.

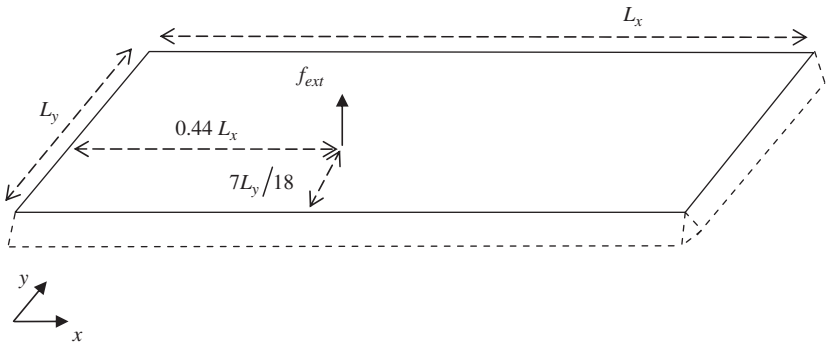


**Fig. 13.** Thin plate with all edges simply supported.

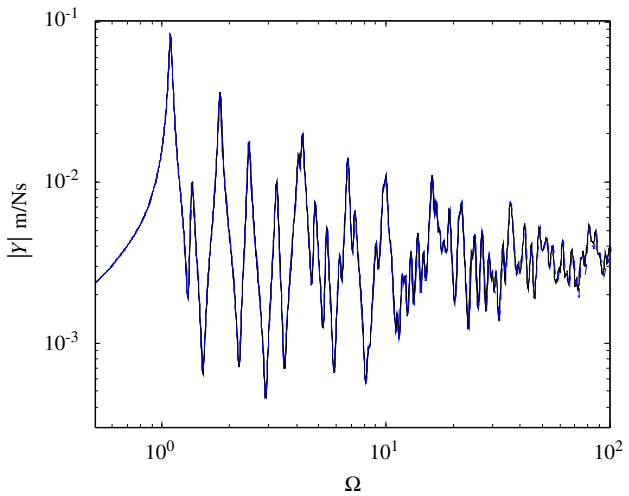


**Fig. 14.** Magnitude of the input mobility: — WFE result with reduced wave basis ($\mathrm{Im}\{|k_x \Delta_x|\}<1$) and excited waves calculated from Eq. (52) and · · · · · modal solution.

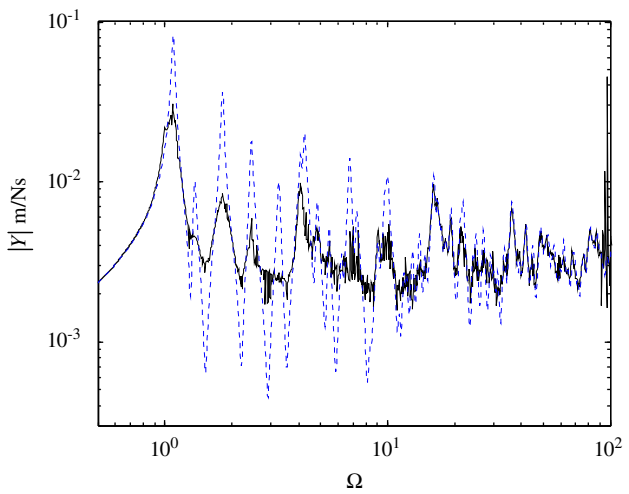


**Fig. 15.** Magnitude of the input mobility of the plate: — WFE result using all wave modes and excited waves calculated from Eq. (52) and · · · · · modal solution.

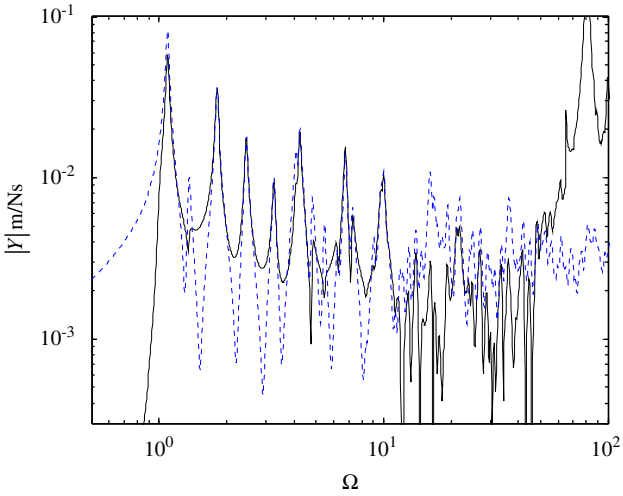


**Fig. 16.** Magnitude of the input mobility of the plate: — WFE result with reduced wave basis ($\mathrm{Im}\{|k_x \Delta_x|\} < 1$) and excited waves calculated from Eq. (49) and · · · · · modal solution.

The contributions of such waves pollute the predicted response. It is therefore important to retain only the wave modes which are predicted reasonably accurately.

Fig. 16 shows the input mobility calculated using the reduced wave basis but with the excited wave amplitudes calculated using the direct matrix inverse in Eq. (43). It can be seen that the results using the original formulation (43) are very inaccurate because of the ill-conditioning. Use of the well-conditioned formulation (45) is therefore necessary.

## 7. Concluding remarks

While analytical solutions exist for the wave behaviour of simple structures, numerical approaches are desirable for complicated structures. One approach is the wave and finite element method. It starts from a finite element (FE) model of only a short segment of the structure. Existing element libraries and commercial FE packages can be fully utilised. Numerical issues arise, however, and these have been discussed in this paper. The emphasis was placed on waveguide structures since these suffer more from numerical problems than do 2-dimensional wave-bearing structures, the FE model potentially being larger. Methods were described to remove or reduce numerical difficulties. Numerical examples were presented.

The eigenvalue problem for free wave propagation can be phrased in a number of ways, the choice depending in part on the form of the desired solution. In summary:

- eigenanalysis of the transfer matrix of the segment (Eq. (8)) is very prone to poor conditioning because it involves both large and small eigenvalues;
- for free wave propagation in undamped structures, the equations of motion can be projected onto the degrees of freedom $\mathbf{q}_L$ of the left hand side of the segment, resulting in the eigenvalue problem of Eq. (13) or (18);
- Zhong's method [22] (Eq. (16)) is recommended: it provides a general, well-posed, form of the eigenvalue problem for real and complex wavenumbers.

Section 3 described various numerical issues. In summary:

- as in conventional FE, there are discretisation errors; furthermore, the spatial discretisation of the structure and the consequent spatial periodicity result in the presence of periodic artefacts: spurious solutions which do not represent wave motion in the continuum. Both of these problems can be avoided if the element size is small enough, typically such that, for the largest wavenumber in the structure, $k\Delta \leq 1$;
- periodic artefacts can be detected by calculating the sensitivity with respect to the element length (Eq. (19));
- if the element length is too small round-off errors due to truncation of inertia terms occur when the dynamic stiffness matrix is calculated. These can be overcome by forming a super-segment from the concatenation of two or more of the segments originally modelled;
- if concatenated segments are used, the internal DOFs can be eliminated by dynamic condensation—Eq. (22)—or, if it is necessary to reduce computational cost, by the approximate scheme described in Eq. (26). Guyan reduction is ineffective;

- problems can arise in the determination of the eigenvectors using Zhong's method, particularly at low frequencies: in Section 3.4 a method based on singular value decomposition was proposed to overcome this problem (Eq. (32)).

Regarding the forced response (Section 5):

- the use of a reduced wave basis removes many problems—in essence the highest order wave modes are excluded;
- direct calculation of the excited wave amplitudes (Eq. (43)) is very prone to poor numerical conditioning: exploiting the orthogonality of the left and right eigenvectors (Eq. (10)) circumvents this problem.

In summary, the WFE method, if properly implemented, provides a powerful tool for the numerical analysis of wave motion in structures. The full power of existing element libraries and commercial FE packages can be fully utilised. The numerical issues that can arise can be handled using the methods described in this paper, including in particular Zhong's method and SVD for the eigenproblem, a reduced wave basis for the modelling, and utilising the orthogonality of the left and right eigenvectors.

## References

[1] K.F. Graff, *Wave Motion in Elastic Solids*, Dover Publications Inc., New York, 1975.
[2] L. Cremer, M. Heckl, B.A.T. Petersson, *Structure-Borne Sound*, third ed., Springer, New York, 2005.
[3] B.R. Mace, D. Duhamel, M.J. Brennan, L. Hinke, Finite element prediction of wave motion in structural waveguides, *Journal of the Acoustical Society of America* 117 (2005) 2835–2843.
[4] D. Duhamel, B.R. Mace, M.J. Brennan, Finite element analysis of the vibration of waveguides and periodic structures, *Journal of Sound and Vibration* 294 (2006) 205–220.
[5] D.J. Thompson, Wheel-rail noise generation part III: rail vibration, *Journal of Sound and Vibration* 161 (1993) 421–446.
[6] L. Gry, C. Gontier, Dynamic modelling of railway track: a periodic model on a generalized beam formulation, *Journal of Sound and Vibration* 199 (1997) 531–558.
[7] L. Houillon, M.N. Ichchou, L. Jezequel, Wave motion in thin-walled structures, *Journal of Sound and Vibration* 281 (2005) 483–507.
[8] M. Maess, N. Wagner, L. Gaul, Dispersion curves of fluid filled elastic pipes by standard FE models and eigenpath analysis, *Journal of Sound and Vibration* 296 (2006) 264–276.
[9] J.M. Mencik, M.N. Ichchou, Wave finite elements in guided elastodynamics with internal fluid, *International Journal of Solids and Structures* 44 (2007) 2148–2167.
[10] J.M. Mencik, M.N. Ichchou, Multi-mode propagation and diffusion in structures through finite elements, *European Journal of Mechanics, A—Solids* 24 (5) (2005) 877–898.
[11] R.M. Orris, M. Petyt, A finite element study of harmonic wave propagation in periodic structures, *Journal of Sound and Vibration* 33 (2) (1974) 223–236.
[12] R.M. Orris, M. Petyt, Random response of periodic structures by a finite element technique, *Journal of Sound and Vibration* 43 (1) (1975) 1–8.
[13] Y.A. Abdel-Rahman, Matrix Analysis of Wave Propagation in Periodic System, PhD Thesis, University of Southampton, 1979.
[14] D.J. Mead, Wave propagation in continuous periodic structures: research contributions from Southampton, 1964–1995, *Journal of Sound and Vibration* 190 (3) (1996) 495–524.
[15] J. Signorelli, A.H. Flotow, Wave propagation, power flow and resonance in a truss beam, *Journal of Sound and Vibration* 126 (1) (1988) 127–144.
[16] M.L. Accorsi, M.S. Bennett, A finite element based method for the analysis of free wave propagation in stiffened cylinders, *Journal of Sound and Vibration* 148 (2) (1991) 279–292.
[17] M.S. Bennett, M.L. Accorsi, Free wave propagation in periodically ring-stiffened shells, *Journal of Sound and Vibration* 171 (1) (1994) 49–66.
[18] M. Ruzzene, F Scarpa, F Soranna, Wave beaming effects in two-dimensional cellular structures, *Smart Materials and Structures* 12 (2003) 363–372.
[19] B.R. Mace, E. Manconi, Modelling wave propagation in two-dimensional structures using finite element analysis, *Journal of Sound and Vibration* 318 (2008) 884–902.
[20] E. Manconi, B.R. Mace, Wave characterisation of cylindrical and curved panels using a finite element method, *Journal of the Acoustical Society of America* 125 (2009) 154–163.
[21] E. Manconi, B.R. Mace, Modelling wave propagation in cylinders using a wave/finite element technique, *Proceeding of the 19th International Congress on Acoustics*, Madrid, 2007.
[22] W.X. Zhong, F.W. Williams, On the direct solution of wave propagation for repetitive structures, *Journal of Sound and Vibration* 181 (1995) 485–501.
[23] M.N. Ichchou, S. Akrout, J.M. Mencik, Guided waves group velocity and energy velocities via finite elements, *Journal of Sound and Vibration* 305 (2007) 931–944.
[24] Y. Waki, On the Application of Finite Element Analysis to Wave Motion in One-Dimensional Waveguides, PhD Thesis, ISVR, University of Southampton, 2007.
[25] M. Petyt, *Introduction to Finite Element Vibration Analysis*, Cambridge University Press, Cambridge, MA, 1990.
[26] L. Brillouin, *Wave Propagation in Periodic Structures*, second ed., Dover, New York, 1953.
[27] W.X. Zhong, G. Cheng, Regularization of singular control and stiffness shifting, *Proceedings of the Asia-Pacific Conference on Computational Mechanics*, Blakema, Rotterdam, 1991, pp. 373–378.
[28] W.X. Zhong, F.W. Williams Wave, Problems for repetitive structures and symplectic mathematics, *Proceedings of the Institution of Mechanical Engineers, Part C* 206 (1992) 371–379.
[29] D.J. Mead, Wave propagation and natural modes in periodic system: I. Mono-coupled systems, *Journal of Sound and Vibration* 40 (1975) 1–18.
[30] D.J. Mead, Wave propagation and natural modes in periodic systems: II. Multi-coupled systems, with and without damping, *Journal of Sound and Vibration* 40 (1975) 19–39.
[31] R.L. Fox, M.P. Kapoor, Rate of change of eigenvalues and eigenvectors, *AIAA* 6 (12) (1968) 2426–2429.
[32] M.I. Friswell, J.E. Mottershead, *Finite Element Model Updating in Structural Dynamics*, Kluwer Academic Publishers, Dordrecht, 1995.
[33] Y. Waki, B.R. Mace, M.J. Brennan, Vibration analysis of a tyre model using the wave finite element method, *19th International Congress on Acoustics*, Madrid, 2007.
[34] B.R. Mace, Wave reflection and transmission in beams, *Journal of Sound and Vibration* 97 (1984) 237–246.
[35] D.W. Miller, A. Flotow, A travelling wave approach to power flow in structural networks, *Journal of Sound and Vibration* 128 (1989) 145–162.
[36] L.S. Beale, M.L. Accorsi, Power flow in two-and three-dimensional frame structures, *Journal of Sound and Vibration* 185 (1995) 685–702.
[37] S.-K. Lee, B.R. Mace, M.J. Brennan, Wave propagation, reflection and transmission in non-uniform waveguides, *Journal of Sound and Vibration* 304 (2007) 31–49.